Acta Crystallographica Section D
Biological Crystallography
ISSN 0907-4449

Crystallization and preliminary crystallographic analysis of *Bacillus subtilis* guanine deaminase

Yu-Jui Chang,[a,b] Chun-Hsiang Huang,[a,c] Chih-Yung Hu[a,c] and Shwu-Huey Liaw[a,c,d,e]*

[a]Structural Biology Program, National Yang-Ming University, Taipei, Taiwan, [b]Institute of Biotechnology in Medicine, National Yang-Ming University, Taipei, Taiwan, [c]Institute of Biochemistry, National Yang-Ming University, Taipei, Taiwan, [d]Faculty of Life Science, National Yang-Ming University, Taipei, Taiwan, and [e]Department of Medical Research and Education, Taipei Veterans General Hospital, Taipei, Taiwan

Correspondence e-mail: shliaw@ym.edu.tw

Received 25 March 2004
Accepted 12 April 2004

Guanine deaminase, a key enzyme in nucleotide metabolism, catalyzes the hydrolytic deamination of guanine to xanthine. The first guanine deaminase crystal from *Bacillus subtilis* was grown in the absence or presence of the inhibitor hypoxanthine in 30% polyethylene glycol 4000, 0.2 *M* ammonium acetate and 0.1 *M* sodium citrate pH 6.5. The crystals belong to space group $C222_1$, with unit-cell parameters $a = 84.91$, $b = 90.90$, $c = 80.19$ Å, with one dimer per asymmetric unit. The crystals diffract X-rays to beyond 1.2 Å resolution and an initial atomic model has been built based on selenomethionyl multiwavelength anomalous data at 2 Å resolution. Unexpectedly, this is the first domain-swapped structure in the cytidine deaminase superfamily.

1. Introduction

Purine/pyrimidine bases and nucleotides not only serve as nitrogen and carbon sources but also participate in nucleotide synthesis. A deamination step is the first and the committed step in the degradation and salvage pathways. Therefore, purine/pyrimidine deaminases play key roles in nucleotide metabolism and become attractive candidates for antibacterial and anticancer therapy.

Guanine deaminase (GD; EC 3.5.4.3) catalyzes the hydrolytic deamination of guanine into xanthine and ammonia. Two types of GDs have evolved separately: the 156-residue *Bacillus subtilis* enzyme belongs to the cytidine deaminase (CDA) superfamily (Nygaard *et al.*, 2000; Ko *et al.*, 2003), while the 454-residue dimeric human counterpart belongs to the TIM-barrel metallohydrolase superfamily (Yuan *et al.*, 1999; Lai *et al.*, 2004). *B. subtilis* GD can be induced with purines as nitrogen sources (Nygaard *et al.*, 2000; Schultz *et al.*, 2001). On the other hand, the tissue-specific expression and developmental changes in the expression of mammalian GDs suggest a potential role in regulation of the guanylate nucleotide pool (Yuan *et al.*, 1999; Kuwahara *et al.*, 1999). GD has been well established as an indicator of hepatocellular diseases, in particular acute hepatitis and hepatoma, because of its near-absence in normal serum (Shiota *et al.*, 1989; Matsunaga *et al.*, 2003; Roberts & Newton, 2004).

The deaminases of the CDA superfamily catalyze the zinc-assisted conversion of the amino group of the cytosine, guanine or adenine moiety into a keto group. To gain structural insight into the substrate specificity and evolution of the enzyme, we have obtained the first GD crystals from *B. subtilis* and have solved the phase problem using the selenomethionyl multiwavelength anomalous dispersion method.

2. Protein preparation, crystallization and X-ray data analysis

The GD gene from *B. subtilis* was expressed using the vector pET-6H in *Escherichia coli* BL21 pLysS (Hsu *et al.*, 2003). The recombinant protein contains eight additional vector residues (MH_6A) at the N-terminus. 3 l Luria broth (LB) cultures were grown at 310 K to an OD_{600} of 0.6 and were induced by the addition of 1 m*M* isopropyl-β-D-thiogalactopyranoside (IPTG). The cells were grown for another 4 h at 310 K before harvesting. Cell pellets were resuspended in 60 ml cold buffer *A* (50 m*M* Tris–HCl, 300 m*M* NaCl pH 8.0) and lysed using a French press. After the removal of cellular debris by centrifugation at 10 000*g* at 277 K for 20 min, the supernatant was applied onto a 5 ml Ni–NTA (Qiagen) column pre-equilibrated with buffer *A*. The resin was washed and the protein was eluted with 20 ml buffer *A* containing 300 m*M* imidazole.

To purify the selenomethionyl-labelled protein, the cells were first incubated in 3 l LB medium at 310 K until an OD_{600} of 0.7 was reached and were then centrifuged at 6000*g* for 15 min. The pellet was washed and suspended in SeMet minimal medium (SeMetMM) and then inoculated into 3 l SeMetMM supplemented with 50 mg l^{-1} seleno-DL-methionine at 298 K for 1 h (Guerrero *et al.*, 2001). After IPTG induction, the cells were grown for another 16 h at 298 K. The selenomethionyl protein was purified in a similar way to the

native protein. SDS–PAGE analysis indicated that the protein was more than 95% pure.

Initial crystallization screening was performed with Hampton Crystal Screens using the hanging-drop vapour-diffusion method at 295 K. The crystals were grown in 30% polyethylene glycol 4000, 0.2 *M* ammonium acetate, 0.1 *M* sodium citrate pH 6.5, using a combination of 2 µl reservoir solution and 2 µl protein solution (30 mg ml^{-1}) in the presence of various amounts (0–20 m*M*) of the transition-state analogue hypoxanthine (Sigma). Crystals could also be obtained using a reservoir solution containing 30% polyethylene glycol monomethyl ether 5000, 0.2 *M* ammonium sulfate, 0.1 *M* MES pH 6.5. Crystals appeared and reached their final dimensions in two weeks at 295 K (Fig. 1). Smaller selenomethionyl crystals with dimensions of 0.4 × 0.2 × 0.02 mm were grown in 30% polyethylene glycol 8000, 0.2 *M* ammonium acetate and 0.1 *M* sodium citrate pH 6.5.

X-ray diffraction data were collected at 100 K without the addition of any other cryoprotectants. The crystals diffracted to 2.0 Å resolution using in-house radiation, but to beyond 1.2 Å resolution using synchrotron radiation. Data were collected using an ADSC Quantum 4 CCD camera at beamlines BL12B2 and BL41XU at SPring-8 and beamlines BL-6A and NW12 at the Photon Factory, Japan. Data were processed using the program *HKL* (Otwinowski & Minor, 1997). The phase problem was solved by multiwavelength anomalous diffraction using selenomethionine as the anomalous diffractor with *SOLVE* and initial dimeric models were built using *RESOLVE* (Terwilliger & Berendzen, 1999).

3. Results and discussion

Autoindexing and the consideration of systematically absent reflections revealed that the crystals belong to the orthorhombic space group $C222_1$, with unit-cell parameters $a = 84.91$, $b = 90.90$, $c = 80.19$ Å. The packing density suggests that there is one dimer per asymmetric unit ($V_M = 2.1$ Å^3 Da^{-1}), with a solvent content of 41%. Both native and selenomethionyl multiple anomalous data have been collected and the data statistics are summarized in Table 1.

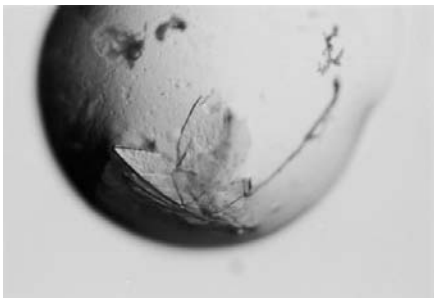

Figure 1
Clusters of *B. subtilis* GD crystals with dimensions of 0.8 × 0.4 × 0.03 mm. These crystals usually cluster together and are very thin and fragile.

Table 1
Statistics for zinc and selenium multiwavelength anomalous data collection.

Values in parentheses are for the highest resolution shell.

	Se peak	Se inflection	Se remote	Zn peak
Wavelength (Å)	0.9798	0.9799	0.9571	1.2813
Resolution (Å)	50–1.51 (1.54–1.51)	50–1.55 (1.58–1.55)	50–2.0 (2.03–2.0)	30–1.9 (1.93–1.90)
Observed reflections	330022	264196	58224	309357
Unique reflections	46806	43936	17470	24554
Completeness (%)	95.3 (74.0)	94.5 (86.1)	81.4 (67.6)	99.7 (99.3)
Average $I/\sigma(I)$	11.0 (2.9)	11.1 (2.7)	8.2 (2.7)	11.0 (6.6)
R_{merge} (%)	7.3 (30.5)	8.7 (35.0)	9.9 (30.9)	10.5 (23.5)

Three Se positions were identified by *SOLVE* based on the selenomethionyl anomalous data with a figure of merit of 0.41 (Fig. 2). An initial dimeric model with 250 polyalanine residues in ten chains was then built by *RESOLVE*. The partial model was subsequently compared with *B. subtilis* CDA (Johansson *et al.*, 2002) and yeast cytosine deaminase (CD; Ko *et al.*, 2003), revealing high structural homology. In addition to the Se peaks, the CDA and CD structures were used to assist in sequential assignment of the ten chains in the model. The twofold non-crystallographic symmetry matrices were subsequently calculated using the *LSQKAB* program from the *CCP*4 package (Collaborative Computational Project, Number 4, 1994) and the matrices were able to improve the model building to a completeness of approximately 95%.

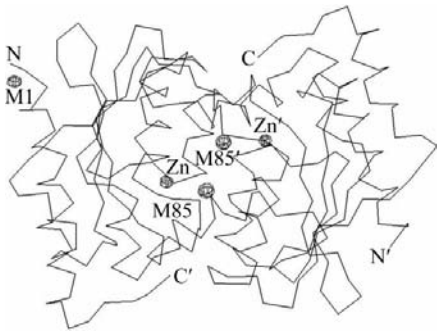

Figure 2
C^{α} trace of the dimeric *B. subtilis* GD, with the Zn and Se anomalous difference Fourier maps contoured at 20σ showing the two zinc and three selenium peaks. There are three methionines in each recombinant subunit: the first residue in the vector linker, together with Met1 and Met85 of the original protein. In the dimer in the asymmetric unit, only Met1 and Met85 in one subunit and Met85′ in the other subunit are ordered.

Based on the Fourier electron-density maps generated by the selenomethionyl and zinc anomalous data, the remaining residues and two zinc ions were introduced into the model using *TURBO-FRODO* (Roussel & Cambillau, 1991). Unexpectedly, the structure revealed domain-swapping of the C-terminal segment. The high-resolution structure should thus provide essential information regarding the structural diversity and the substrate specificity in the CDA superfamily. Structural refinement is still in progress and a full description of the refined structure will be published elsewhere.

The synchrotron-radiation experiments were performed at the National Synchrotron Radiation Research Center, Taiwan, at the Photon Factory (Proposal No. 2002 G309), Japan and at SPring-8 with the approval of the Japan Synchrotron Radiation Research Institute (Proposal No. 2003B1004-CNL1-np). This study was supported by National Science Council Grant NSC 92-2320-B-010-071.

References

Collaborative Computational Project, Number 4 (1994). *Acta Cryst.* D**50**, 760–763.
Guerrero, S. A., Hecht, H. -J., Hofmann, B., Biebl, H. & Singh, M. (2001). *Appl. Microbiol. Biotechnol.* **56**, 718–723.
Hsu, Y.-H., Hu, C.-Y., Lin, J- J. & Liaw, S.-H. (2003). *Acta Cryst.* D**59**, 950–952.
Johansson, E., Mejlhede, N., Neuhard, J. & Larsen, S. (2002). *Biochemistry*, **41**, 2563–2570.
Ko, T.-P., Lin, J.-J., Hu, C.-Y., Hsu, Y.-H., Wang, A. H.-J. & Liaw, S.-H. (2003). *J. Biol. Chem.* **278**, 19111–19117.
Kuwahara, H., Araki, N., Makino, K., Masuko, N., Honda, S., Kaibuchi, K., Fukunaga, K., Miyamoto, E., Ogawa, M. & Saya, H. (1999). *J. Biol. Chem.* **274**, 32204–32214.
Lai, W.-L., Chou, L.-Y., Ting, C.-Y., Kirby, R., Tsai, Y.-C., Wang, A. H.-J. & Liaw, S.-H. (2004). *J. Biol. Chem.* **279**, 13962–13967.
Matsunaga, H., Honda, H., Kubo, K., Sannomiya, K., Cui, X., Toyota, Y., Mori, T., Muguruma, N., Okahisa, T., Okamura, S., Shimizu, I. & Ito, S. J. (2003). *Med. Invest.* **50**, 64–71.
Nygaard, P., Bested, S. M., Andersen, K. A. K. & Saxild, H. H. (2000). *Microbiology*, **146**, 3061–3069.

Otwinowski, Z. & Minor, W. (1997). *Methods Enzymol.* **276**, 307–326.
Roberts, E. L. & Newton, R. P. (2004). *Anal. Biochem.* **324**, 250–257.
Roussel, A. & Cambillau, C. (1991). *Silicon Graphics Geometry Partners Directory*, p. 86. Mountain View, CA, USA: Silicon Graphics.
Schultz, A., Nygaard, P. & Saxild, H. H. (2001). *J. Bacteriol.* **183**, 3293–3302.
Shiota, G., Fukada, J., Ito, T., Tsukizawa, M., Yamada, M. & Sato, M. (1989). *Jpn J. Med.* **28**, 22–24.
Terwilliger, T. C. & Berendzen, J. (1999). *Acta Cryst.* D**55**, 849–861.
Yuan, G., Bin, B. C., McKay, D. J. & Snyder, F. F. (1999). *J. Biol. Chem.* **274**, 8175–8180.